

RADIOGRAPHY CAPABILITIES FOR MATTER-RADIATION INTERACTIONS IN EXTREMES*

P. L. Walstrom[#], R. W. Garnett, R. L. Barber, J. A. O'Toole, T. S. Gomez, C. A. Chapman, H. R. Salazar, Los Alamos National Laboratory, Los Alamos, New Mexico 87545

Abstract

The Matter-Radiation Interactions in Extremes (MaRIE) experimental facility [1] will be used to discover and design the advanced materials needed to meet 21st century national security and energy security challenges. This new facility will provide the new tools scientists need to develop next-generation materials that will perform predictably and on-demand for currently unattainable lifetimes in extreme environments. The MaRIE facility is based on upgrades to the existing LANSCE 800-MeV proton linac and a new 12-GeV electron linac and associated X-ray FEL to provide simultaneous multiple probe beams, and new experimental areas. In addition to the high-energy photon probe beam, both electron and proton radiography capabilities will be available at the MaRIE facility. Recently, detailed radiography system studies have been performed to develop conceptual layouts of high-magnification electron and proton radiography systems that can meet the experimental requirements for the expected first experiments to be performed at the facility. A description of the radiography systems, their performance requirements, and a proposed facility layout are presented.

FACILITY MISSION

The mission need is to provide qualification, certification, and assessment of materials in the nuclear deterrent stockpile. Material interfaces, defects, and microstructure between the scales of atomic structure and the engineering continuum (the so-called mesoscale) determine time-dependent properties, from shock response to manufacturing processes to aging. Test samples will be synthesised and characterized at the mesoscale, and their dynamic behavior in time-dependent extreme conditions characterized by use of both imaging and diffractive scattering with multiple probes at multiple spatial and time scales.

FACILITY OVERVIEW

The MaRIE facility (see Fig. 1) will be built on the TA-53 site at LANL and will make use of the existing 800-MeV proton linac. New facility components include a 12-GeV electron linac, 42-keV X-ray FEL/undulator, X-ray, electron, and proton beam lines, new experimental halls, and materials fabrication/characterization facilities. X-ray, electron, and proton beams intersect in multibeam radiography areas or hutches (see Fig. 2).

*Work supported by US Department of Energy, Office of National Nuclear Security Administration. Contract No. DE-AC52-06NA25396.
[#] walstrom@lanl.gov

12-GeV Superconducting Electron Linac

The choice of a superconducting (SC) linac was driven by the requirement of having up to 30 microbunches over a time window of up to 100 μ s, which rules out high-gradient normal-conducting structures [2]. The SC linac will use the same basic 1.3-GHz cavities as planned for the European XFEL and LCLS-II. The design assumes a cavity accelerating gradient of 31.5 MV/m. The total length of the linac is 750 m, which gives it an average (real-estate) gradient of 16 MV/m.

Undulator

The undulator is a hybrid permanent magnet type with an on-axis field of 0.7 T and a period of 1.86 cm. The total undulator length is 138 m. There are 28 undulator segments and 16 FODO periods, each with a length of 8.6 m. Two of the FODO periods contain chicanes and monochromators for seeding.

FEL Undulator and X-Ray Beam Transport

In the initial stage of the facility, a single undulator/FEL will be used to produce a bright, coherent X-ray beam of up to 42 keV energy with a photon flux in excess of 2×10^{10} photons in each 30-fs pulse. Silicon kinoform lenses are used to expand the x-ray beam. Bragg scattering from crystals is used to deflect the X-ray beam at small angles of up to 5 degrees into multiple X-ray beamlines. Another set of kinoform lenses, labelled "objectives", then focus the expanded X-ray beam onto the targets with different focused spot radii, depending on the experimental requirements.

12-GeV Electron and 800-MeV Proton Radiography Systems

Proton radiography (pRad) is a mature technology, with systems operating in the USA, Germany, and Russia. Electron radiography (eRad) in the GeV range is under development [3], with proof-of-principle experiments planned for the summer of 2015 at SLAC. Both eRad and pRad have the same basic system components, but the physics of beam interaction with objects differs: ionization energy loss and multiple Coulomb scattering (MCS) are nearly the same for both eRad and pRad, but bremsstrahlung energy loss is important in eRad and negligible for pRad, and nuclear scattering is important for pRad but small for eRad. Bremsstrahlung energy loss limits 12-GeV eRad of high-Z materials (U, Pu, etc.) to thicknesses of a few millimeters or less. Object thicknesses in 800-MeV pRad are limited by MCS, dE/dx energy loss, and second-order lens chromatic aberrations. Both techniques use matching illuminating beams, point-

Content from this work may be used under the terms of the CC BY 3.0 licence (© 2015). Any distribution of this work must maintain attribution to the author(s), title of the work, publisher, and DOI.



Figure 1: Layout of the MaRIE Facility in TA-53.

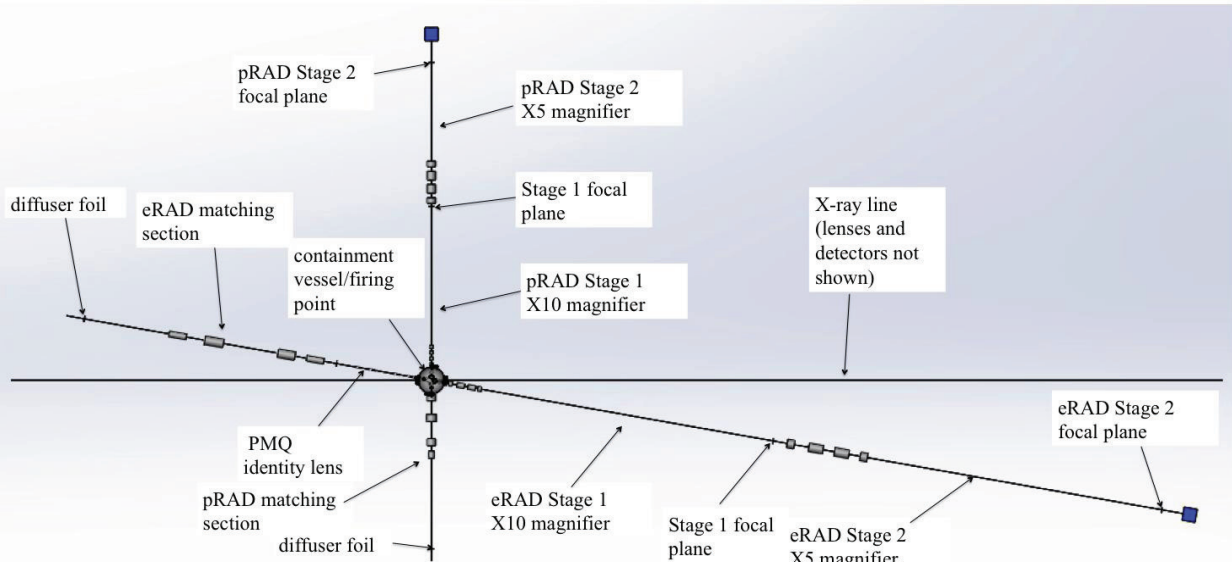


Figure 2: Layout of MaRIE multi-beam radiography area.

to-point imaging with quadrupole magnetic lenses, and get image contrast by the use of angle cuts on the MCS distribution; in pRad contrast due to inelastic nuclear scattering out of the lens/collimator acceptance adds to the angle-cut contrast. With electron bunches of less than picosecond length, motion blur is negligible in comparison to other resolution limiting effects, such as lens aberrations, detector pixel size, etc.

Both eRad and pRad systems start with a diffuser foil and matching system of quadrupole magnets and drifts, followed by the test object, quadrupole magnetic lenses, and imaging detector. For high-magnification imaging (up to a magnification of 50), a two-stage lens, in which the second stage magnifies the real image formed by the first stage, will be used (see Fig. 3). In order to reduce bremsstrahlung background in eRad, an achromatic bend can be used to deflect the image away from the forward bremsstrahlung spot. This is done by centering a weak dipole magnet at the focal plane of the first stage/image plane of the second stage. In MaRIE, the test object will be placed in a chamber where electron, x-ray and proton beams pass through the object.

At present, for both eRad and pRad, the imaging detector consists of a scintillator viewed by multiple fast digital cameras. Frame-to-frame time spacing is limited

by the scintillator light decay time (~ 40 ns for LSO and a few ns for plastics); individual frame times are determined by the beam bunch lengths, typically less than 0.1 ps for eRad and FEL X-rays and about 100 ps for pRad.

Chromatically Matched Beams and Angle Cuts

The use of matched beams to eliminate certain second-order chromatic aberrations was an important early discovery of the LANL pRAD program [4]. With perfect focus settings and elimination of quadrupole field errors (e.g. roll errors, sextupole components, etc.), the most important remaining lens aberrations are 2nd-order chromatic aberrations, although 3rd-order geometric aberrations (caused by angled trajectories in quadrupoles, not field errors) can also be significant in large-field-of-view systems. The 3rd-order aberrations can be corrected with octupoles [5]. The matching section expands and tilts the upright beam ellipse just after the diffuser foil such that at the object the $x-x'$ and $y-y'$ distributions are almost line distributions, with $x'=k_x x$ and $y'=k_y y$. Denoting the 2nd-order chromatic-aberration coefficients by T_{116} , T_{126} , T_{336} , and T_{346} , it is shown in Ref. [4] that if we set $k_x = -T_{116}/T_{126}$ and $k_y = -T_{336}/T_{346}$, the aberrations due to T_{116} and T_{336} vanish, leaving only the second-order terms $T_{126}\phi_x$

and $T_{346}\phi_y$, where ϕ_x and ϕ_y are the x - and y -plane scattering angles in the object. The effect of these remaining second-order aberrations on image quality is both object and beam-dependent, since they involve the product of an energy spread and an angular spread. For sufficiently thin objects in eRad (objects much thinner than a radiation length), the energy spread after the object is dominated by the beam energy spread; normally the angular spread is dominated by scattering in the object, not the illuminating beam emittance.

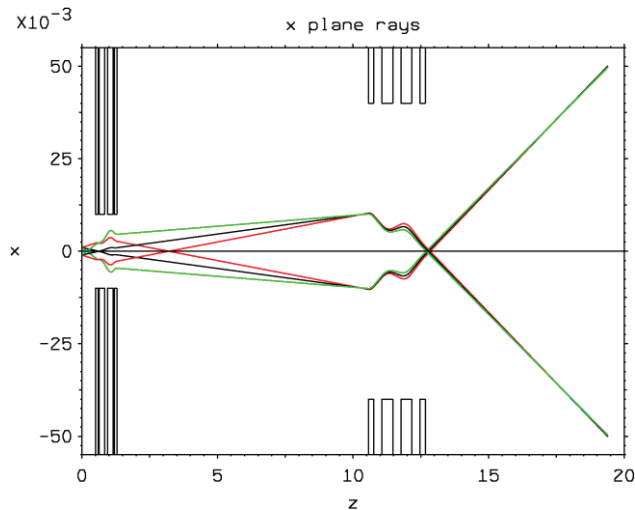


Figure 3: Matched and scattered rays in a $\times 50$ compound lens. Black: matched; red: positively scattered ray, green: negatively scattered ray.

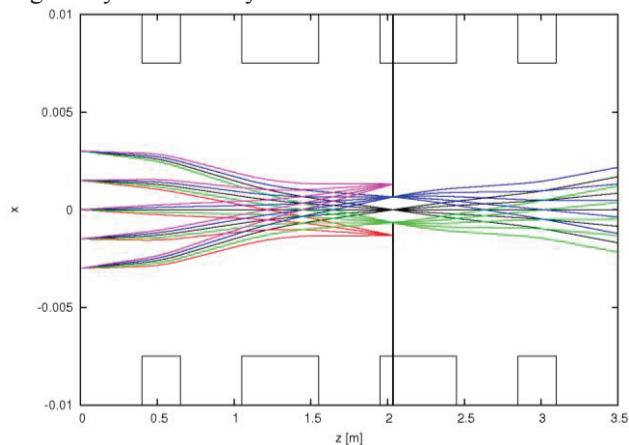


Figure 4: Angle cuts and matched rays in the x plane for a single-stage $\times 10$ lens. Quadrupoles are indicated by the rectangles. Black curves: matched rays, no scattering; colored curves: scattered rays. The angle-cut collimator is represented by the vertical bars in the 3rd quadrupole.

The matching coefficients k_x and k_y depend on the lens, are both negative for magnifying lenses, and are generally larger in magnitude with greater lens magnifications. Angle cuts are made at the points in the lens (Fourier points) where the conditions $R_{11}(z)+k_x R_{12}(z)=0$, $R_{33}(z)+k_y R_{34}(z)=0$ are met; the z values for the x and y Fourier planes can be different and sometimes fall within quadrupoles (see Fig. 4). If the Fourier points are widely

separated, individual x and y slit-type collimators can be used. Aberration-limited resolution of better than 0.1 micron in thin objects should be possible with 12 GeV eRAD (see Fig. 5); real resolution will be worse due to non-ideal collimator behavior (problematic for the small scattering angles associated with thin objects), finite detector pixel size, image statistics, and background. Finite pixel-size effects can be mitigated by increasing magnification.

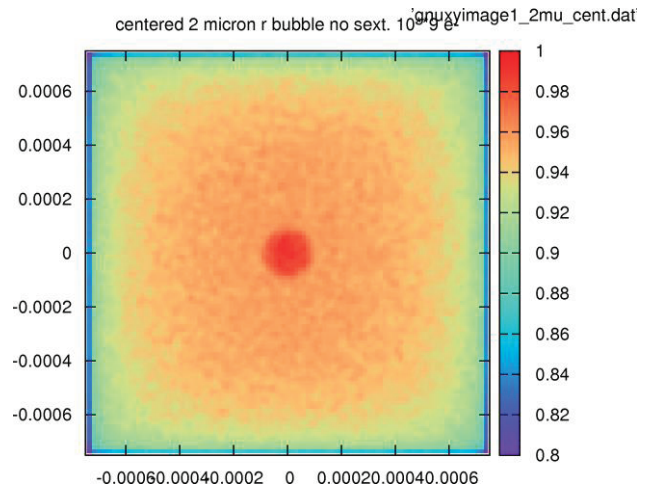


Figure 5: False-color simulated 12 GeV eRAD image of a 2 micron radius bubble in a 100 micron thick U slab, using a $\times 50$ magnifier. Pixel size is approximately 0.2 microns (referred to the object). A “zoomed” 20×20 flat-intensity rectangular beam was used to improve image statistics, which are better than with typical eRAD single bunches and a ~ 1 millimeter FOV; the fall-off of image intensity at the border is an artifact.

REFERENCES

- [1] C. W. Barnes, J. L. Barber, E. M. Kober, T. Lookman, R. L. Sandberg, J. Shlachter, and R. L. Sheffield, “MaRIE 1.0: The Matter-Radiation Interactions in Extremes Project, and the Challenge of Dynamic Mesoscale Imaging”, LA-UR-15-21334, Feb. 2, 2015.
- [2] R. L. Sheffield, “Enabling Cost-Effective High-Current Burst-Mode Operation in Superconducting Accelerators”, Nuclear Instruments and Methods in Physics Research A 785 (2015) 197–200.
- [3] F. Merrill, F. Harmon, A. Hunt, F. Mariam, K. Morley, C., Morris a, A. Saunders, and C. Schwartz, “Electron Radiography”, Nuclear Instruments and Methods in Physics Research B 261 (2007) 382–386.
- [4] C. T. Mottershead and J. D. Zumbro, “Magnetic Optics for Proton Radiography, Proc. US Particle Accelerator Conference, Vol. 2, May 12-16, 1997, pp. 1397-1399.
- [5] P. L. Walstrom, “Geometric Aberrations in AHF Quadrupole Lenses”, Los Alamos internal report LA-UR-01-4638, August, 2001.